Role of molecular alignment in attosecond photoionization of N_2

Ru Zhang,[1] Feng Wang,[1,*] Qing Liao,[1,†] and Peixiang Lu[1,2]

[1]*Hubei Key Laboratory of Optical Information and Pattern Recognition, Wuhan Institute of Technology, Wuhan 430205, China*

[2]*Guangdong Intelligent Robotics Institute, Dongguan 523808, China*

(Received 20 November 2022; revised 17 April 2023; accepted 6 July 2023; published 20 July 2023)

We theoretically study the influence of molecular alignment on the attosecond photoionization of the N_2 molecule. Based on the numerical simulations of the single-active-electron two-dimensional time-dependent Schrödinger equation, we find that the alignment-averaged photoelectron momentum distributions deviate from the single-molecule result, especially for a large molecular alignment angle and a low degree of molecular alignment. As a result, the photoemission time delays extracted from the angular-averaged streaking spectra are different from the single-molecule result. More importantly, the alignment-averaged photoemission time delays are found to depend on the degree of molecular alignment as well as the molecular alignment distribution. Our results reveal the important role of molecular alignment in the molecular attosecond photoionization.

DOI: 10.1103/PhysRevA.108.013113

I. INTRODUCTION

The development of attosecond extreme ultraviolet (xuv) pulses based on high-order harmonic generation (HHG) in gases has opened the possibility for the observation and control of electron dynamics in atoms, molecules, and solids [1]. When an attosecond xuv pulse interacts with mediums, many dramatic phenomena occur. Single-photon ionization is one of the most fundamental processes. The photoelectron momentum distributions (PEMDs) generated in the single-photon ionization process carry the structure information of the mediums, which has been used to image molecular orbitals [2].

However, the attosecond pump-probe technique by using an attosecond xuv and infrared (ir) pulses, such as the attosecond streaking [3–7] and reconstruction of attosecond beating by interference of two-photon transitions (RABBIT) [8–10], can measure photoemission time delay. The photoemission time delay can advance our understanding of different electronic dynamics. In general, the photoemission time delay of atoms retrieved from the streaking spectrum can be decomposed into the Eisenbud-Wigner-Smith delay [11] and the Coulomb-laser coupling time delay [12–14]. The first is simply the derivative of the phase of the photoionization dipole matrix element with respect to energy $t_{\mathrm{EWS}} = \frac{d}{dE}\arg\langle\varphi_{\mathbf{p}}(\mathbf{r})|\mathbf{r}\cdot\mathbf{n}|\psi_i(\mathbf{r})\rangle$ with $\psi_i(\mathbf{r})$ the initial-state wave function and $\varphi_{\mathbf{p}}(\mathbf{r})$ the final wave function. $\mathbf{r}$ is the position operator and $\mathbf{n}$ denotes the polarization direction of the electric field. The second originates from the exit-channel interactions of the outgoing electron with a Coulombic long-range tail. For the photoionization of degenerate hydrogenic manifolds where dipolar interactions are present in the entrance channel, the photoemission time delay is further modified by the dipole-laser coupling effect [15,16]. For the many-electron atoms, the electron-electron interaction is also reported to contribute to the photoemission time delay [16–19]. Moreover, the emission-angle dependence of the photoemission time delay has also been studied [20–22].

Compared to atoms, the molecules have a complex internal structure which will give rise to more complex PEMD. Some other effects, such as the two-center interference [23–25], the shape resonance [26–29], and the structure of molecules [30–33], can induce additional contributions to the photoemission time delay of molecules. Moreover, the influences of directions of the molecular axis and the emitted electron on the attosecond photoionization of molecules have also attracted wide attention [34,35]. However, the partially aligned molecules usually show different angular distributions at the different degrees of alignment.

In this work, we study the effect of molecular alignment on the single-photon ionization of the N_2 molecule. The single-active-electron (SAE) two-dimensional (2D) time-dependent Schrödinger equation (TDSE) is adopted to calculate the single-molecule PEMD and photoemission time delay. Based on our simulations, we find a significant influence of the alignment average effect on the molecular PEMD and photoemission time delay. The alignment-averaged PEMD and photoemission time delay are demonstrated to be far different from the single-molecule result.

This paper is structured as follows. In Sec. II, we introduce the numerical methods in our calculations, including the solution of TDSE of single-molecule (Sec. II A) and the nonadiabatic field-free molecular alignment (Sec. II B). Section III shows the numerical results of single-molecule and alignment-averaged PEMDs and photoemission time delays. A summary is presented in Sec. IV. Atomic units are used throughout this paper unless otherwise stated.

II. THEORETICAL MODEL

A. Single-molecule PEMDs

We first calculate the single-molecule PEMD by solving the SAE 2D-TDSE [36,37]. In the TDSE, the elec-

*wangfeng@wit.edu.cn
†liaoqing@wit.edu.cn

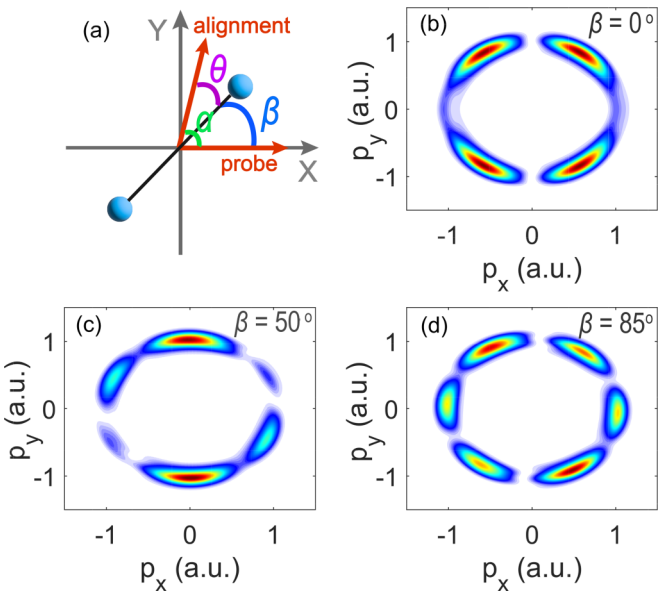

FIG. 1. (a) Sketch of the geometry of molecular alignment in our simulation. (b) The single-molecule PEMD of the N_2 molecule with an angle β of 0°. (c), (d) Same as (b), but for the angle β of 50° and 85°. Here, the photon energy of the xuv pulse $\omega_{\rm xuv} = 30$ eV.

tronic wave packets are generated from an initial wave function $\Psi(\mathbf{r}, t_0)$ by

$$\Psi(\mathbf{r}, t) = U_H(t, t_0)\Psi(\mathbf{r}, t_0), \tag{1}$$

with U_H being the unitary time evolution operator satisfying the TDSE

$$i\frac{\partial}{\partial t}U_H(t, t_0) = H(\mathbf{r}, t)U_H(t, t_0), U_H(t_0, t_0) = 1, \tag{2}$$

with a SAE-Hamiltonian $H(\mathbf{r}, t)$, which is given by

$$H(\mathbf{r}, t) = -\tfrac{1}{2}\nabla^2 + V_C(\mathbf{r}) + V_L(\mathbf{r}, t), \tag{3}$$

where $V_L(\mathbf{r}, t) = \mathbf{r}\cdot\mathbf{F}(t)$ is the interaction of the electron with the laser field. $\mathbf{F}(t)$ is the electric field. $V_C(\mathbf{r})$ is the effective single-active-electron potential of the N_2 molecule [37]

$$V_C(\mathbf{r}) = \sum_{n=1}^{2}\frac{-Z_n(\mathbf{r})}{\sqrt{|\mathbf{r}|^2 + a_n^2}}. \tag{4}$$

The position-dependent effective charge is

$$Z_n(\mathbf{r}) = Z_n^{\infty} + \left(Z_n^0 - Z_n^{\infty}\right)e^{\left(-\frac{|\mathbf{r}-\mathbf{u}_n|^2}{\sigma_n^2}\right)}. \tag{5}$$

$n = 1$, 2 labels the nuclei at fixed position $\mathbf{u}_n \equiv [(-1)^n\frac{r_c}{2}\cos\beta, (-1)^n\frac{r_c}{2}\sin\beta]$. Here, r_c is the internuclear distance of the molecule and β is the angle between the molecular axis and polarization direction of the probe pulse as shown in Fig. 1(a). $\mathbf{r} \equiv (x, y)$ denotes the position coordinate of the electron. For the N_2 molecule, the soft Coulomb potential parameter $a_n = 1.2$. $Z_n^{\infty} = 0.5$ is the effective nuclear charge of the nucleus n as seen by an electron at infinite distance. $Z_n^0 = 7$ is the bare charge of nucleus n. $\sigma_n = 0.7$ represents the degree of attenuation of the effective charge of the nucleus with distance and is introduced to account for distance-dependent electron-electron screening effects. The initial state $\Psi(x, y, 0)$ of Eq. (1) is taken as the highest occupied molecular orbital (HOMO) of the N_2 molecule, which is obtained by integrating the time-dependent Schrödinger equation (2) in imaginary time using the split-operator technique [36]. Starting with an arbitrary trial initial wave function of appropriate symmetry and requiring this wave function to remain normalized, the propagated wave function will converge to the lowest-energy state of the same symmetry, the excited components dying off exponentially [38].

Then we solve Eq. (2) in real time by the split-operator method on a Cartesian grid. The entire space is split into the inner ($0 \to R_c$) and outer ($R_c \to R_{\rm max}$) regions by a splitting function at any given time t_i [39],

$$\begin{aligned}\Psi(t_i) &= \Psi(t_i)[1 - F_s(R_c)] + \Psi(t_i)F_s(R_c)\\ &= \Psi_1(t_i) + \Psi_2(t_i).\end{aligned} \tag{6}$$

Here, $F_s(R_c) = 1/[1 + e^{-(r-R_c)/\Delta}]$, R_c is the radius of the boundary separating those two regions, and Δ is the width of the crossover region. Ψ_1 represents the wave function in the inner region which is numerically propagated under the full Hamiltonian, and Ψ_2 represents the wave function in the outer region which is analytically propagated under the Volkov Hamiltonian. When the laser field is over, the final wave function in the outer region is the Fourier transformation of the wave function in momentum space $C(\mathbf{p}, t_i)$,

$$\Psi_2(\infty, t_i) = \int C(\mathbf{p}, t_i)\frac{e^{i\mathbf{p}\cdot\mathbf{r}}}{2\pi}d^2\mathbf{p}. \tag{7}$$

Here, $\mathbf{p}$ is the electron final momentum. Therefore, the single-molecule PEMD is related to the sum of the wave function in momentum space over t_i,

$$\frac{d^2\xi(\mathbf{p})}{dEd\theta_e} = \left|\sum_{t_i} C(\mathbf{p}, t_i)\right|^2, \tag{8}$$

where E is the electron energy associated with $\mathbf{p}$ as $E = |\mathbf{p}|^2/2$ and θ_e is the angle of the emitted electron.

It is worth mentioning that the SAE 2D-TDSE model used in our simulations does not include the continuum electron dynamics and also neglects other effects, such as electron correlation, which might play a role in photoionization time delay. This limits the applicability of our method for predicting or simulating experimental outcomes. However, in this work, the primary objective is to gain a deeper understanding of the influence of molecular alignment on photoionization time delay, not to simulate or predict the outcome of an experiment. Therefore, the SAE 2D-TDSE approach used here remains reasonable. Moreover, it also offers a means to disentangle the impact of molecular alignment from other known sources of photoemission time delay, some of which are absent in our simplified model.

B. Nonadiabatic field-free molecular alignment

In this section, we introduce the calculation model of the molecular alignment. The molecular alignment can be created in both the adiabatic and nonadiabatic manners, which is mainly determined by the duration of the alignment pulse

[40,41]. When the duration of the alignment pulse is long compared to the rotational periods of the molecule, each eigenstate of the field-free Hamiltonian is guaranteed to evolve adiabatically into the corresponding state of the complete Hamiltonian during the turn-on, returning to the original (isotropic) field-free eigenstate upon turn-off. While, when the duration of alignment pulse is much shorter than the rotational period, the nonadiabatic alignment plays an important role. In this case, the alignment pulse prepares the molecule in a coherent superposition of rotational eigenstates that dephases and rephases field-freely afterwards. As a consequence, recurrence of alignment or antialignment appears at the rotational revivals. Here, we adopt an alignment pulse with the duration of 50 fs to align the molecules. The duration of the alignment pulse is much shorter than the rotation period of the N_2 molecule $T_{\rm rev} = \frac{1}{2B_e c} = 8.4$ ps, where B_e is the rotational constant of the N_2 molecule and c is the velocity of light. The induced molecular alignment is nonadiabatic. As shown in Fig. 1(a), the angle between the polarization directions of the alignment and probe pulses is defined as α. The angle between the polarization directions of the alignment pulse and molecular axis is θ. For the case of the single-molecule response, or namely, the perfect alignment, the molecular axis is along the polarization direction of the alignment pulse, i.e., $\theta = 0^o$ and then $\alpha = \beta$.

In the molecular alignment model, the time-dependent molecular angular distribution $\rho(\theta, \phi, t')$ can be written as a weighted average of the squared modulus of the time-dependent rotational wave packet $\psi_{JM}(\theta, \phi, t')$, i.e.,

$$\rho(\theta, \phi, t') = \sum_{JM} \Gamma_{JM} |\psi_{JM}(\theta, \phi, t')|^2, \tag{9}$$

where ϕ is the azimuthal angle in the frame of the alignment pulse. Note that, imposed by the linearly polarized alignment pulse, the resulting rotational wave packet has a cylindrical symmetry in space, thus $\rho(\theta, \phi, t')$ is independent of the azimuthal angle ϕ. Γ_{JM} is the population of the initial state $|JM\rangle$ given by the Boltzmann distribution. The time-dependent rotational wave packet $\psi_{JM}(\theta, \phi, t')$ can be obtained by solving the TDSE of the molecular rotational wave packet [40,41]

$$i\frac{\partial \psi_{JM}(\theta, \phi, t')}{\partial t'} = \left[B_e J^2 - \frac{\epsilon(t')^2}{4}(\alpha_\parallel \cos^2\theta + \alpha_\perp \sin^2\theta)\right]\psi_{\rm JM}(\theta, \phi, {\rm t}'). \tag{10}$$

Here, $\epsilon(t')$ is the electric field of the alignment pulse, $\alpha_\parallel$ and $\alpha_\perp$ are the parallel and perpendicular components of the polarizability tensor. For the N_2 molecule, $B_e = 1.989$ cm^{-1}, $\alpha_\parallel = 4.05$ Å^3, and $\alpha_\perp = 1.45$ Å^3 [42]. Equation (10) can be solved with the split-operator method. The degree of alignment is calculated by

$$\langle \cos^2\theta \rangle(t') = \sum_{JM} \Gamma_{JM} \langle \psi_{JM}(\theta, \phi, t') | \cos^2\theta | \psi_{JM}(\theta, \phi, t') \rangle. \tag{11}$$

Finally, by the coherent superposition of the final wave function in momentum space weighted by the molecular angular distribution $\rho(\theta, t')$, we can obtain the angular-averaged PEMDs at different time delays τ between the xuv and ir pulses and different time delays t' between the

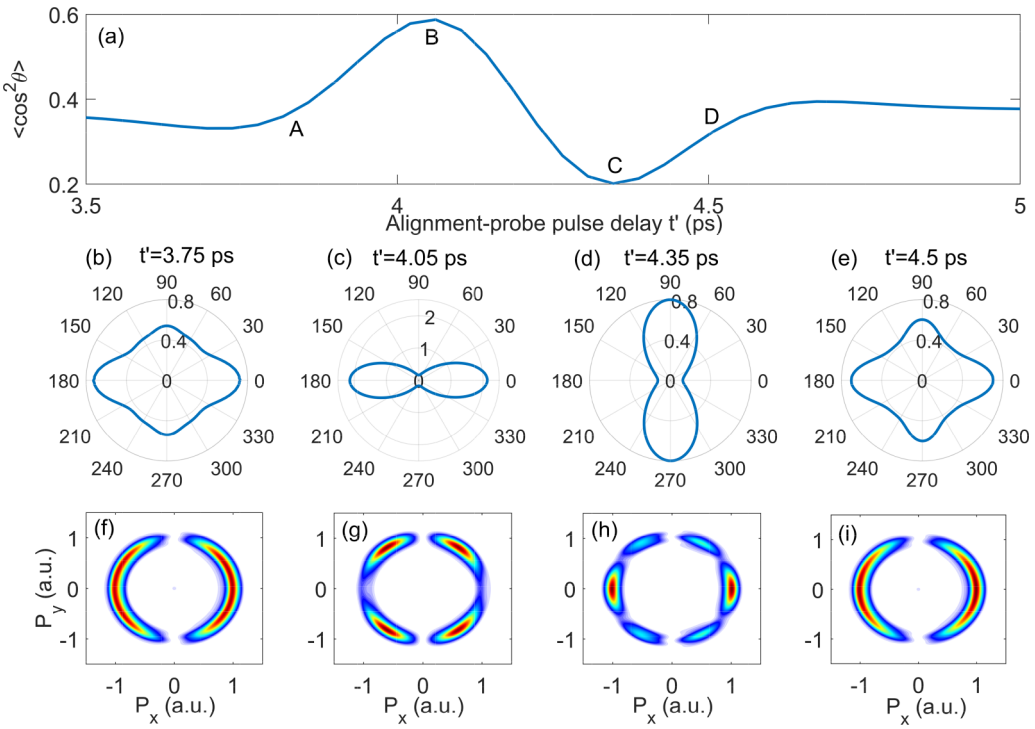

FIG. 2. (a) Evolution of the alignment factor $\langle \cos^2\theta \rangle$ with alignment-probe pulse delay. [(b)–(e)] The angular distribution of the N_2 molecule at the time delays of 3.75, 4.05, 4.35, and 4.5 ps, respectively. Here the angle α is 0°. [(f)–(i)] Angular-averaged PEMDs of the N_2 molecule at the same time delays in [(b)–(e)]. Here, $\omega_{\rm xuv} = 30$ eV.

alignment and probe pulses

$$P_e(\mathbf{p}, t', \tau) = \int \sum_{t_i} C(\mathbf{p}, t_i, \beta, \tau)\rho(\theta, t')d\theta. \quad (12)$$

Then we can obtain the angular-averaged streaking spectrum by taking the τ-dependent angular-averaged PEMDs along the positive x direction.

III. RESULTS AND DISCUSSIONS

In Fig. 1, we show the calculated single-molecule PEMDs of the N_2 molecule for different polarization angles β between the molecular axis and the polarization direction of the probe pulse. In our calculation, we adopt a 400-as xuv pulse with the intensity of 1×10^{12} W/cm^2 as probe pulse. The xuv pulse is polarized along the x direction. The photon energy of the xuv pulse is 30 eV. For different angles β, we rotate the polarization direction of molecular axis in the X-Y plane. Figures 1(b) to 1(d) plot the PEMDs of the N_2 molecule calculated for three specific angles β of 0°, 50°, and 85°. One can see that the PEMDs depend sensitively on the angle β. Specifically, when the N_2 molecule is aligned along the polarization direction of the xuv pulse (i.e., $\beta = 0°$), the PEMD exhibits a four-lobe structure as shown in Fig. 1(b). While for the angle β of 50° and 85° [Figs. 1(c) and 1(d)], the PEMDs are more complex. In Fig. 2, we study the influence of the alignment average effect on the PEMDs of the N_2 molecule. As shown in Fig. 1(a), in our calculations, an alignment pulse with moderate intensity and polarizing angle α is first applied to create molecular alignment in the X-Y plane. The alignment pulse prepares the molecule in a coherent superposition of rotational eigenstates that dephases and rephases. For the linear molecule of N_2, the alignment is reconstructed periodically at multiples of the rotational period $T_{\rm rev}$. In general, the degree of alignment can be represented by the alignment factor $\langle\cos^2\theta\rangle$. In Fig. 2(a), we calculate the time evolution of the alignment factor $\langle\cos^2\theta\rangle$ of the N_2 molecule. Here, the intensity, wavelength and duration of the alignment pulse are 5×10^{13} W/cm^2, 800 nm, and 50 fs, respectively. The alignment pulse is linearly polarized along the x axis. The molecular rotational temperature is 50 K. One can see that $\langle\cos^2\theta\rangle$ shows strong delay dependence at the half rotational revivals, e.g., $t' = 4.2$ ps, and reaches a maximum ($\langle\cos^2\theta\rangle = 0.6$) at $t' = 4.05$ ps. For the other time, the molecule will have different angular distributions. For example, in Figs. 2(b) to 2(e), we plot the angular distribution of the N_2 molecule at 3.75, 4.05, 4.35, and 4.5 ps, which are marked as A, B, C, and D in Fig. 2(a). At $t' = 4.05$ ps (point B), the molecules are temporarily well confined in a narrow angle around the polarization direction of the alignment pulse [see Fig. 2(c)]. Then the angular-averaged PEMD presents a four-lobe structure [Fig. 2(g)], which is similar to the single-molecule result in Fig. 1(b). At $t' = 4.35$ ps (point C), the alignment factor $\langle\cos^2\theta\rangle$ reaches a minimum, which means that the most molecules were perpendicular to the polarization direction of the alignment pulse [Fig. 2(d)]. Then the angular-averaged PEMD presents a six-lobe structure [Fig. 2(h)]. At $t' = 3.75$ ps (point A) and $t' = 4.5$ ps (point D), the N_2 molecule is nearly randomly aligned ($\langle\cos^2\theta\rangle = 0.33$) [Figs. 2(b) and 2(e)], the angular-averaged PEMDs present a two-lobe structure [Figs. 2(f) and 2(i)], which is similar to the PEMD generated by an atom [43].

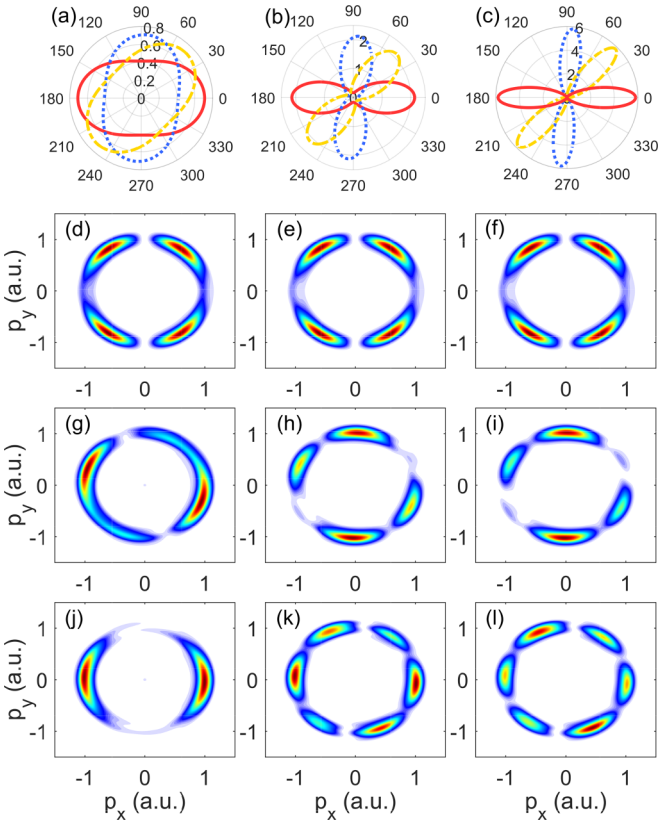

FIG. 3. [(a)–(c)] The angular distribution of the N_2 molecule at $t' = 4.05$ ps for different alignment degrees $\langle\cos^2\theta\rangle$ of 0.4, 0.6, and 0.8. The red, yellow, and blue lines are the results for different angle α of 0°, 50°, and 85°. [(d)–(f)] Angular-averaged PEMDs of the N_2 molecule for different alignment degree of 0.4, 0.6, and 0.8. Here, α is 0°. [(g)–(i)] and [(j)–(l)] Same as [(d)–(f)], but for α of 50° and 85°, respectively. Here $\omega_{\rm xuv} = 30$ eV.

The degree of alignment can be controlled by the intensity of the alignment pulse. We then plot the angular distribution at the time delay of $t' = 4.05$ ps for different intensities of the alignment pulse of 1×10^{13} W/cm^2, 5×10^{13} W/cm^2, and 7×10^{13} W/cm^2 in Figs. 3(a) to 3(c), respectively. The $\langle\cos^2\theta\rangle$ at $t' = 4.05$ ps in Figs. 3(a) to 3(c) are equal to 0.4, 0.6, and 0.8, respectively. The red, yellow, and blue lines in Figs. 3(a) to 3(c) are for the N_2 molecule primarily aligned at 0°, 50°, and 85°, respectively. As shown in Figs. 3(d) to 3(f), for $\alpha = 0°$, the angular-averaged PEMDs for different degrees of alignment present in a four-lobe structure, which is similar to the single-molecule result in Fig. 1(b). While, for a large alignment angle, e.g., $\alpha = 50°$ [Figs. 3(g) to 3(i)] and 85° [Figs. 3(j) to 3(l)], the angular-averaged PEMDs deviate from the single-molecule results [Figs. 1(c) to 1(d)]. This deviation is more serious for lower degrees of alignment, such as $\langle\cos^2\theta\rangle = 0.4$ in Figs. 3(g) and 3(j) and 0.6 in Figs. 3(h) and 3(k).

In Fig. 4, we study the photoemission time delay $\delta\tau$ in the N_2 molecule. First, we consider the single-molecule result. To extract the photoemission time delay $\delta\tau$, we calculate the single-molecule attosecond streaking spectrum. The

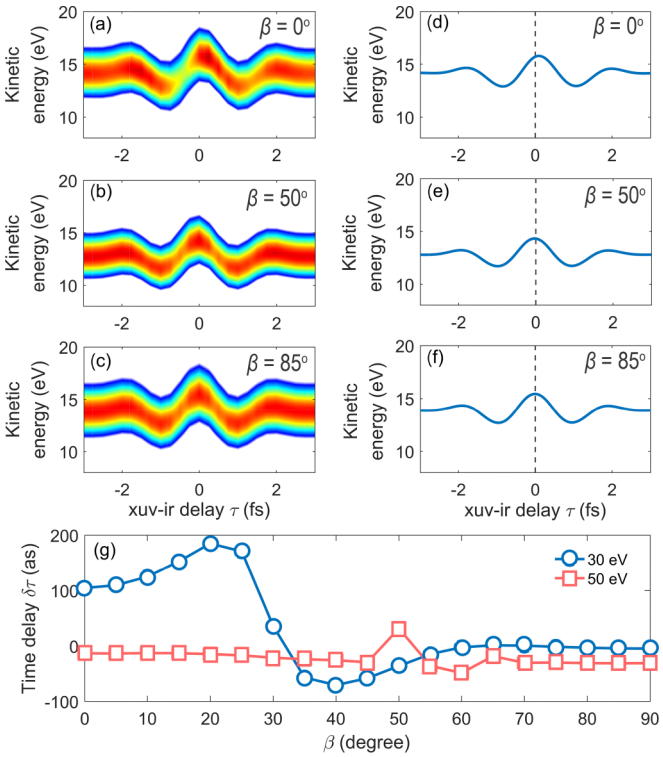

FIG. 4. [(a)–(c)] The attosecond streaking spectra of single N_2 molecule for different polarization angle β of 0°, 50° and 85°. [(d)–(f)] The corresponding COEs of the streaking spectra. Here, ω_{xuv} = 30 eV. (g) The photoemission time delay $\delta\tau$ of single N_2 molecule as a function of β for ω_{xuv} of 30 and 50 eV, respectively.

single-molecule attosecond streaking spectrum is obtained by recording a set of single-molecule PEMDs over a range of delays τ between the xuv and ir pulses. In the calculation, the parameters of the xuv pulse are the same as that in Figs. 1 to 3. The intensity, wavelength, and duration of the ir field are 5×10^{11} W/cm^2, 600 nm, and 3 T_0 (T_0 is the optical cycle of the ir field). The ir streaking field is polarized along the x direction. Figures 4(a) to 4(c) are the attosecond streaking spectra in the positive x direction for the polarization angle β of 0°, 50°, and 85°. Here, ω_{xuv} = 30 eV. To extract the photoemission time delay, we calculated the center of energies (COEs) of sthe treaking spectrum in Figs. 4(d) to 4(f). The COEs are defined as

$$E_{\mathrm{COE}}(\tau) = \frac{\int E P_E(E, \theta_e = 0, \tau) dE}{\int P_E(E, \theta_e = 0, \tau) dE}, \tag{13}$$

where θ_e is the emission angle of the electron. By fitting the COEs of the streaking spectrum into an analytic function with the same form as the vector potential of the ir field, i.e., $aA_{ir}(\tau - \delta\tau) + b$, we obtain the photoemission time delay $\delta\tau$. In Fig. 4(g), we show the photoemission time delay $\delta\tau$ as a function of the polarization angle β for ω_{xuv} of 30 eV (line with circles). One can see that the $\delta\tau$ at ω_{xuv} of 30 eV depends sensitively on the β. Specifically, $\delta\tau$ is positive for $\beta < 30°$ and becomes negative in the range from 30° to 60°. For $\beta > 60°$, $\delta\tau$ is close to zero. Moreover, we also show $\delta\tau$ at ω_{xuv} of 50 eV (line with squares), which also depends on

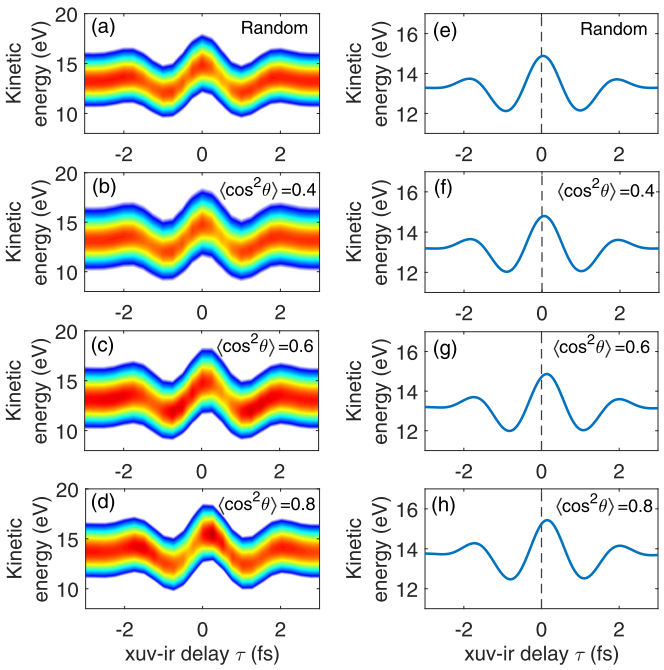

FIG. 5. [(a)–(d)] The angular-averaged attosecond streaking spectra of the N_2 molecule for random alignment, alignment degrees of 0.4, 0.6, and 0.8. [(e)–(h)] The corresponding COEs of the streaking spectra. Here the α is 0° and ω_{xuv} = 30 eV.

the β. But $\delta\tau$ at ω_{xuv} of 50 eV is very small when compared to that at ω_{xuv} of 30 eV.

We next study the influence of the alignment average effect on the photoemission time delay. In Figs. 5(a) to 5(d), we calculated the angular-averaged attosecond streaking spectra for several different degrees of alignment. Here, the molecule is primarily aligned at $\alpha = 0°$ and ω_{xuv} = 30 eV. The angular-averaged attosecond streaking spectrum is obtained by calculating the averaged PEMDs as a function of the delay between the xuv and ir pulses. The corresponding COEs of the streaking spectra are presented in Figs. 5(e) to

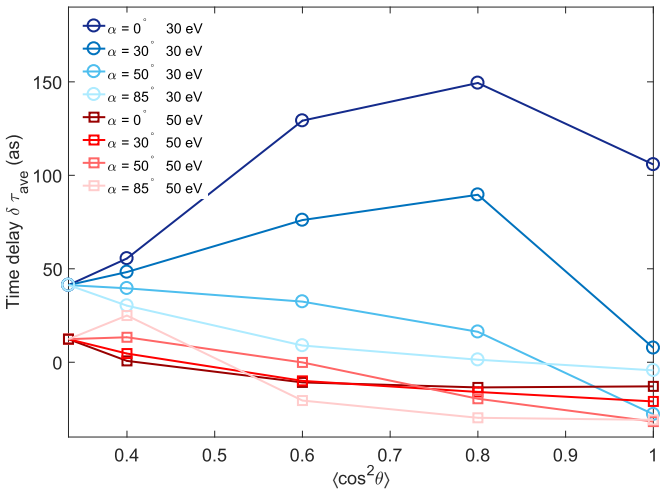

FIG. 6. The photoemission time delay $\delta\tau_{ave}$ as a function of alignment degree for α of 0°, 30°, 50°, and 85° at ω_{xuv} = 30 and 50 eV.

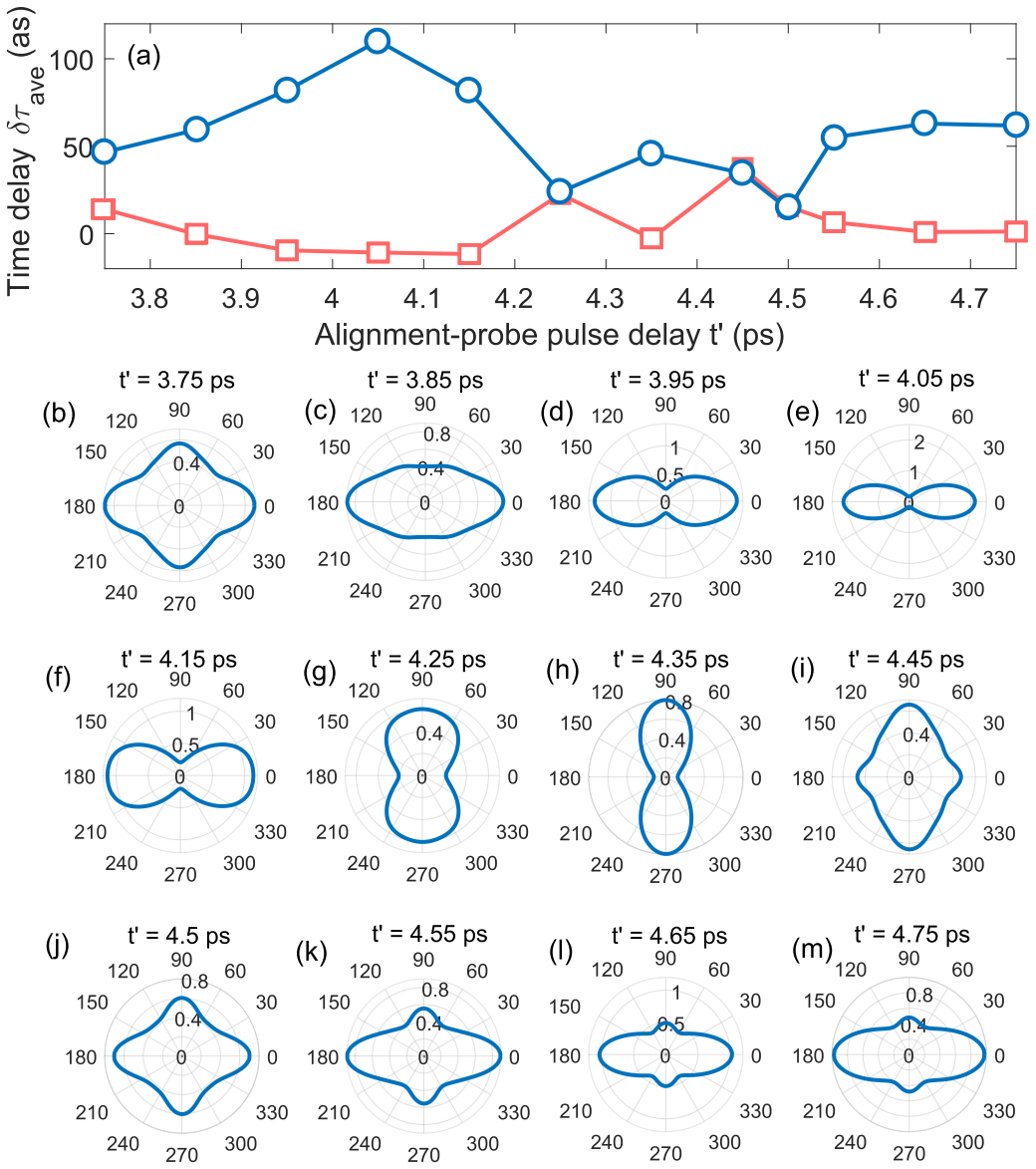

FIG. 7. (a) The photoemission time delay $\delta\tau_{ave}$ as a function of the time delay t' between the alignment and probe pulses for the ω_{xuv} of 30 and 50 eV, respectively. [(b)–(m)] The angular distribution of the N_2 molecule at different time delays t'. Here, the angle α is 0° and $\omega_{xuv} = 30$ eV. The parameter of the alignment pulse is the same as that in Fig. 2.

5(h). We further extract the angular averaged photoemission time delay $\delta\tau_{ave}$ in Fig. 6. In addition, we also calculated $\delta\tau_{ave}$ for $\alpha = 30°$, 50°, and 85°. One can see that the alignment degree-dependent averaged time delay $\delta\tau_{ave}$ are different from the single-molecule result ($\langle\cos^2\theta\rangle = 1$ in Fig. 6. The dependence of $\delta\tau_{ave}$ on the degree of alignment can be qualitatively understood from the angular distribution of the N_2 molecule in Figs. 3(a) to 3(c) and the single-molecule $\delta\tau$ in Fig. 4(g). For example, for $\alpha = 0°$, for a low degree of alignment, e.g., random alignment or $\langle\cos^2\theta\rangle = 0.4$ [Fig. 3(a)], the N_2 molecules have a broad angle distribution in space. The N_2 molecules aligned at large angle with negative time delay $\delta\tau$ [Fig. 4(g)] will make the considerable contribution to the $\delta\tau_{ave}$. Thus, the resulting $\delta\tau_{ave}$ is much smaller than the single-molecule result. With the increase of degree of alignment, the angular distribution of the N_2 molecule becomes narrow [Figs. 3(b) and 3(c)]. The contribution of molecules aligned at large angle is reduced, which leads to the increase of $\delta\tau_{ave}$. Specifically, at the degree of alignment of 0.8 [Fig. 3(c)], the molecules have a large probability to align around $\theta = 20°$, where the single-molecule $\delta\tau$ is maximum. In this case, the averaged $\delta\tau_{ave}$ is larger than the single-molecule result, and after $\langle\cos^2\theta\rangle = 0.8$, $\delta\tau_{ave}$ decreases. Likewise, the results in Fig. 6 for α of 30°, 50°, and 85° can be understood in a similar way. Moreover, we also show the angular-averaged photoemission time delay $\delta\tau_{ave}$ with ω_{xuv} 50 eV in Fig. 6. One can see that the result also presents a dependence on the degree of alignment, but also the smaller values of $\delta\tau$ compared to that with $\omega_{xuv} = 30$ eV.

In Fig. 7(a), we calculated the angular-averaged photoemission time delay $\delta\tau_{ave}$ at the different alignment-probe pulse delays t' for ω_{xuv} of 30 (line with circles) and 50 eV (line with squares), respectively. Meanwhile, we also show the corresponding angular distributions of the N_2 molecule in

Figs. 7(b) to 7(m). The parameter of the alignment pulse is the same as that in Fig. 2. One can see that the molecular angular distribution also has a significant effect on $\delta\tau_{\rm ave}$.

In our TDSE simulations, the time delay extracted from the molecular PEMD includes the Wigner time and the Coulomb-laser coupling-effect-induced time delay. If only the Wigner time is considered, the photoemission delay is simply the derivative of the phase of the photoionization dipole matrix element with respect to energy $\delta\tau = \frac{d}{dE}\arg[d_x(p_x,\beta)]$, $d_x(p_x,\beta) = \langle\varphi_{p_x}(\mathbf{r})|x|\psi_i(\mathbf{r},\beta)\rangle$ with $\psi_i(\mathbf{r},\beta)$ the HOMO orbital of N_2 at different polarization angle β and $\varphi_{p_x}(\mathbf{r})$ the final state. Considering the alignment average effect, the photoemission delay then becomes $\delta\tau_{\rm ave} = \frac{d}{dE}\arg[\int \rho(\theta)\cdot d_x(p_x,\beta)\sin\theta d\theta]$. The $\rho(\theta)$ is energy independent, thus $\delta\tau_{\rm ave} = \int \rho(\theta)\cdot\frac{d}{dE}\arg[d_x(p_x,\beta)]\sin\theta d\theta = \int \rho(\theta)\cdot\delta\tau(\beta)\sin\theta d\theta$. In this case, the angular-averaged photoemission time delay $\delta\tau_{\rm ave}$ can be approximated as a sum of the angle-resolved single-molecule time delays $\delta\tau(\beta)$ weighted by the molecular angular distribution $\rho(\theta)$.

Moreover, it is worth noting that, when using a broadband xuv pulse to illuminate the N_2 molecule, due to the small energy gap between the HOMO and HOMO-1 orbitals, the electrons of HOMO and HOMO-1 orbitals can be simultaneously ionized and generate the vibrational wavepacket. The vibrational wavepacket indeed will affect the time delay. However, in our simulation, we adopt a single-active-electron TDSE to calculate the PEMDs and attosecond streaking spectra, which does not include the contribution of the HOMO-1 orbital. Even when the contribution of the HOMO-1 orbital is considered, the obtained PEMD and photoelectron time delay will be different, but the effect of molecular alignment on the photoelectron time delay in molecules can still hold. Likewise, when using the Fourier instead of Coulomb waves, the value of the single-molecule time delay will be different from our TDSE calculations. However, the influence of molecular alignment on time delay will still exist.

IV. CONCLUSION

In summary, we studied the impact of molecular alignment on the attosecond photoionization of the N_2 molecule. The numerical results of SAE 2D-TDSE show that the molecular alignment effect plays an important role in the generation of molecular PEMDs, especially for a large molecular alignment angle and a low degree of molecular alignment. Further, we found that the molecular alignment effect can induce an additional contribution to the molecular photoemission time delay, and it is different for different degrees of molecular alignment as well as the molecular alignment distributions. Our results reveal that the molecular alignment average effect plays an important role in the attosecond photoionization of molecules.

ACKNOWLEDGMENTS

This work was supported by Guangdong Major Project of Basic and Applied Basic Research (Grant No. 2019B030302003), National Natural Science Foundation of China under Grants No. 12104349 and No. 12174295, and the Campus Science Foundation Research Project of Wuhan Institute of Technology, China (Grant No. K2021076).

[1] F. Krausz and M. Ivanov, Rev. Mod. Phys. **81**, 163 (2009).
[2] P. Salières, A. Maquet, S. Haessler, J. Caillat, and R. Taïeb, Rep. Prog. Phys. **75**, 062401 (2012).
[3] E. Constant, V. D. Taranukhin, A. Stolow, and P. B. Corkum, Phys. Rev. A **56**, 3870 (1997).
[4] J. Itatani, F. Quéré, G. L. Yudin, M. Y. Ivanov, F. Krausz, and P. B. Corkum, Phys. Rev. Lett. **88**, 173903 (2002).
[5] M. Drescher, M. Hentschel, R. Kienberger, G. Tempea, C. Spielmann, G. A. Reider, P. B. Corkum, and F. Krausz, Science **291**, 1923 (2001).
[6] F. Wang, Z. Xiong, X. Zhang, Q. Liao, and P. Lu, Opt. Express **29**, 39729 (2021).
[7] F. Wang, Q. Liao, K. Liu, M. Qin, X. Zhang, Q. Zhang, W. Cao, L. W. Pi, Y. Zhou, and P. Lu, Phys. Rev. A **103**, 013115 (2021).
[8] V. Véniard, R. Taïeb, and A. Maquet, Phys. Rev. A **54**, 721 (1996).
[9] P. M. Paul, E. S. Toma, P. Breger, G. Mullot, F. Auge, P. Balcou, H. G. Muller, and P. Agostini, Science **292**, 1689 (2001).
[10] C. Palatchi, J. M. Dahlström, A. S. Kheifets, I. A. Ivanov, D. M. Canaday, P. Agostini, and L. F. DiMauro, J. Phys. B **47**, 245003 (2014).
[11] P. A. Martin, Time delay of quantum scattering processes, in *New Developments in Mathematical Physics. Acta Physica Austriaca*, edited by H. Mitter and L. Pittner (Springer, Vienna, 1981), Vol. 23.
[12] O. Smirnova, M. Spanner, and M. Y. Ivanov, J. Phys. B **39**, S323 (2006).
[13] C. H. Zhang and U. Thumm, Phys. Rev. A **82**, 043405 (2010).
[14] M. Ivanov and O. Smirnova, Phys. Rev. Lett. **107**, 213605 (2011).
[15] S. Nagele, R. Pazourek, J. Feist, K. Doblhoff-Dier, C. Lemell, K. Tökési, and J. Burgdörfer, J. Phys. B **44**, 081001 (2011).
[16] J. C. Baggesen and L. B. Madsen, Phys. Rev. Lett. **104**, 043602 (2010).
[17] M. Schultze *et al.*, Science **328**, 1658 (2010).
[18] S. Sukiasyan, K. L. Ishikawa, and M. Ivanov, Phys. Rev. A **86**, 033423 (2012).
[19] M. Isinger, R. J. Squibb, D. Busto, S. Zhong, A. Harth, D. Kroon, S. Nandi, C. L. Arnold, M. Miranda, J. M. Dahlström, E. Lindroth, R. Feifel, M. Gisselbrecht, and A. L'Huillier, Science **358**, 893 (2017).
[20] S. Heuser, Á. J. Galán, C. Cirelli, C. Marante, M. Sabbar, R. Boge, M. Lucchini, L. Gallmann, I. Ivanov, A. S. Kheifets, J. M. Dahlström, E. Lindroth, L. Argenti, F. Martín, and U. Keller, Phys. Rev. A **94**, 063409 (2016).
[21] C. Cirelli, C. Marante, S. Heuser, C. L. Petersson, Á. J. Galán, L. Argenti, S. Zhong, D. Busto, M. Isinger, S. Nandi, S. MacLot, L. Rading, P. Johnsson, M. Gisselbrecht, M. Lucchini, L. Gallmann, J. M. Dahlström, E. Lindroth, A. L'Huillier, F. Martín, and U. Keller, Nat. Commun. **9**, 955 (2018).
[22] P. Hockett, J. Phys. B **50**, 154002 (2017).

[23] V. V. Serov and A. S. Kheifets, Phys. Rev. A **93**, 063417 (2016).
[24] H. Cohen and U. Fano, Phys. Rev. **150**, 30 (1966).
[25] Q.-C. Ning, L.-Y. Peng, S.-N. Song, W.-C. Jiang, S. Nagele, R. Pazourek, J. Burgdörfer, and Q. Gong, Phys. Rev. A **90**, 013423 (2014).
[26] J. Caillat, A. Maquet, S. Haessler, B. Fabre, T. Ruchon, P. Salières, Y. Mairesse, and R. Taïeb, Phys. Rev. Lett. **106**, 093002 (2011).
[27] S. Nandi, E. Plésiat, S. Zhong, A. Palacios, D. Busto, M. Isinger, L. Neoričić, C. L. Arnold, R. J. Squibb, R. Feifel, P. Decleva, A. L'Huillier, F. Martín, and M. Gisselbrecht, Sci. Adv. **6**, eaba7762 (2020).
[28] X. Gong, W. Jiang, J. Tong, J. Qiang, P. Lu, H. Ni, R. Lucchese, K. Ueda, and J. Wu, Phys. Rev. X **12**, 011002 (2022).
[29] F. Holzmeier, J. Joseph, J. C. Houver, M. Lebech, D. Dowek, and R. R. Lucchese, Nat. Commun. **12**, 7343 (2021).
[30] P. Hockett, E. Frumker, D. M. Villeneuve, and P. B. Corkum, J. Phys. B: At. Mol. Opt. Phys. **49**, 095602 (2016).
[31] A. Chacón and C. Ruiz, Opt. Express **26**, 4548 (2018).
[32] Y. Liao, Y. Zhou, L. W. Pi, Q. Ke, J. Liang, Y. Zhao, M. Li, and P. Lu, Phys. Rev. A **104**, 013110 (2021).
[33] S. Beaulieu, A. Comby, A. Clergerie, J. Caillat, D. Descamps, N. Dudovich, B. Fabre, R. Géneaux, F. Légaré, S. Petit, B. Pons, G. Porat, T. Ruchon, R. Taeb, V. Blanchet, and Y. Mairesse, Science **358**, 1288 (2017).
[34] J. Vos, L. Cattaneo, S. Patchkovskii, T. Zimmermann, C. Cirelli, M. Lucchini, A. Kheifets, A. S. Landsman, and U. Keller, Science **360**, 1326 (2018).
[35] D. Baykusheva and H. J. Wörner, J. Chem. Phys. **146**, 124306 (2017).
[36] M. D. Feit, J. A. Fleck, Jr., and A. J. R. Steiger, J. Comput. Phys. **47**, 412 (1982).
[37] M. Peters, T. T. Nguyen-Dang, E. Charron, A. Keller, and O. Atabek, Phys. Rev. A **85**, 053417 (2012).
[38] K. T. R. Davies, H. Flocard, S. Krieger, and M. S. Weiss, Nucl. Phys. A **342**, 111 (1980).
[39] X. M. Tong, K. Hino, and N. Toshima, Phys. Rev. A **74**, 031405(R) (2006).
[40] H. Stapelfeldt and T. Seideman, Rev. Mod. Phys. **75**, 543 (2003).
[41] E. Péronne, M. D. Poulsen, C. Z. Bisgaard, H. Stapelfeldt, and T. Seideman, Phys. Rev. Lett. **91**, 043003 (2003).
[42] C. Jin, A. T. Le, S. F. Zhao, R. R. Lucchese, and C. D. Lin, Phys. Rev. A **81**, 033421 (2010).
[43] L. R. Moore, M. A. Lysaght, J. S. Parker, H. W. van der Hart, and K. T. Taylor, Phys. Rev. A **84**, 061404(R) (2011).